



**HAL**  
open science

## Monitoring diclofenac adsorption by organophilic alkylpyridinium bentonites

D. B. França, Pollyana Trigueiro, E.C. Silva Filho, M. G. Fonseca, M. Jaber

► **To cite this version:**

D. B. França, Pollyana Trigueiro, E.C. Silva Filho, M. G. Fonseca, M. Jaber. Monitoring diclofenac adsorption by organophilic alkylpyridinium bentonites. *Chemosphere*, 2019, 242, pp.125109. 10.1016/j.chemosphere.2019.125109 . hal-02344483

**HAL Id: hal-02344483**

**<https://hal.sorbonne-universite.fr/hal-02344483v1>**

Submitted on 4 Nov 2019

**HAL** is a multi-disciplinary open access archive for the deposit and dissemination of scientific research documents, whether they are published or not. The documents may come from teaching and research institutions in France or abroad, or from public or private research centers.

L'archive ouverte pluridisciplinaire **HAL**, est destinée au dépôt et à la diffusion de documents scientifiques de niveau recherche, publiés ou non, émanant des établissements d'enseignement et de recherche français ou étrangers, des laboratoires publics ou privés.

1                 **Monitoring diclofenac adsorption by organophilic alkylpyridinium**  
2   **bentonites**

3                     D.B. França<sup>a,b</sup>, P. Trigueiro<sup>c</sup>, E.C. Silva Filho<sup>c</sup>, M.G. Fonseca<sup>a,b</sup>, M. Jaber<sup>d</sup>

4  
5  
6  
7  
8  
9  
10  
11  
12  
13  
14  
15  
16  
17  
18  
19  
20  
21  
22  
23

<sup>a</sup>*Universidade Federal da Paraíba, Cidade Universitária, s/n - Castelo Branco III, 58051-085, João Pessoa - PB, Brazil.*

<sup>b</sup>*Núcleo de Pesquisa e Extensão - Laboratório de Combustíveis e Materiais (NPE – LACOM).*

<sup>c</sup>*Laboratório Interdisciplinar de Materiais Avançados (LIMAV), Centro de Tecnologia, UFPI, Teresina, Piauí, Brazil, 64064-260.*

<sup>d</sup>*Sorbonne Université, Laboratoire d'Archéologie Moléculaire et Structurale, CNRS UMR 8220, Tour 23, 3ème étage, couloir 23-33, BP 225, 4 place Jussieu, 75005 Paris, France.*

24 \*Corresponding author: [mgardennia@quimica.ufpb.br](mailto:mgardennia@quimica.ufpb.br)

25 Phone/fax +55(83) 3216-7441

26 **Abstract**

27 Organoclays have been applied as efficient adsorbents for pharmaceutical pollutants from  
28 aqueous solution. In this work, dodecylpyridinium chloride (C<sub>12</sub>pyCl) and  
29 hexadecylpyridinium chloride (C<sub>16</sub>pyCl) cationic surfactants were used for the preparation of  
30 organobentonites destined for diclofenac sodium (DFNa) adsorption, an anionic drug widely  
31 detected in wastewater. The organofunctionalization of the clay samples was performed under  
32 microwave irradiation at 50 °C for 5 min with surfactant amounts of 100% and 200% in  
33 relation to the cation exchange capacity (CEC) of the pristine bentonite. The amount of  
34 incorporated ammonium salts based on CHN elemental analysis was higher for all samples  
35 prepared with 200% of the CEC. The basal spacings of the organoclays ranged from 1.54-  
36 2.13 nm, indicating the entrance of organic cations into the interlayer spacing of the clay  
37 samples, and the spacing depended on the size of the alkyl organic chain. The hydrophobic  
38 character of the organobentonites was verified by thermogravimetry and infrared  
39 spectroscopy (FTIR). The adsorption isotherms showed that the drug capacity adsorption was  
40 influenced by the amount of surfactant incorporated into the bentonite, the packing density  
41 and the arrangement of the surfactants in the interlayer spacing. Zeta potential measurements  
42 of the organobentonites and FTIR analysis after drug adsorption suggested that electrostatic  
43 and nonelectrostatic interactions contributed to the mechanism of adsorption.

44

45

46

47 **Keywords:** Organobentonite; microwave heating; adsorption; anti-inflammatory drug;  
48 diclofenac

49           **1. Introduction**

50           The presence of pharmaceutical compounds in the environment has become a major  
51 concern, particularly due to the consequences related to long exposure, which are still  
52 unknown (Lonappan et al., 2016). Diclofenac (2- [2,6-dichlorophenylamino] phenylethanoic  
53 acid) is among the main drugs studied in recent years. Diclofenac is a nonsteroidal anti-  
54 inflammatory drug often prescribed in human and veterinary medicine and used to reduce  
55 inflammation and pains (Acuña et al., 2015; He et al., 2017). As a consequence of its high  
56 production and consumption worldwide, both diclofenac and its metabolites have been  
57 detected in aquatic bodies in several countries at concentrations of 0.7-4400 ng L<sup>-1</sup> in surface  
58 waters and up to 8.5 µg L<sup>-1</sup> in wastewater (Lonappan et al., 2016; Scheurell et al., 2009);  
59 concentrations of its transformation products are in the range of 0.08 to 1.80 µg L<sup>-1</sup> (Scheurell  
60 et al., 2009). In Brazil, diclofenac was also observed in water in the range of 3.3-785 ng L<sup>-1</sup>  
61 (Starling et al., 2019). Therefore, diclofenac is among the main drugs studied in recent years  
62 regarding its identification/detection in aquatic bodies (Biel-Maeso et al., 2018; Starling et al.,  
63 2019), removal/degradation (Maia et al., 2019; Mugunthan et al., 2018), and environmental  
64 impacts (Klaudia et al., 2019; Moreno-González et al., 2016; Oaks et al., 2004).

65           Both toxicity and bioaccumulation of diclofenac have been observed for various living  
66 aquatic organisms, even at low concentrations (Klaudia et al., 2019; Moreno-González et al.,  
67 2016), and diclofenac was identified as the cause of mortality and decline of the vulture  
68 population in Pakistan (Oaks et al., 2004). Some studies have observed that diclofenac  
69 metabolites can be generated through biotransformation in living organisms or through  
70 exposure to sunlight, and some of them are even more toxic than pure diclofenac (Bonnefille  
71 et al., 2018; Klaudia et al., 2019).

72           Due to the environmental problems, several diclofenac removal methods have been  
73 evaluated, such as coagulation, flocculation and activated sludge treatment (Carballa et al.,

74 2005; Vieno and Sillanpää, 2014); adsorption based on natural or synthetic materials (Andrew  
75 Lin et al., 2015; Maia et al., 2019); and degradation through advanced oxidative processes,  
76 such as ozonation (Beltrán et al., 2009), photo-Fenton (Pérez-Estrada et al., 2005) and  
77 photocatalysis (Mugunthan et al., 2018).

78 In this context, adsorption is highlighted because of the ease of operation and  
79 avoidance of subproducts. Organophilic clay minerals have been applied as efficient  
80 adsorbents for drug removal from aquatic bodies (Ghemit et al., 2019; Karaman et al., 2012;  
81 Maia et al., 2019; Martinez-Costa et al., 2018; Oliveira et al., 2017; Oliveira and Guégan,  
82 2016; Sun et al., 2017a; Thanhmingliana, 2015). The performance of organophilic clays was  
83 attributed to a better compatibility with organic pollutants thanks to their hydrophobic nature  
84 and to the presence of new sites for adsorption (Oliveira and Guégan, 2016; Zhuang et al.,  
85 2019, 2018). Therefore, modified clays with surfactants containing an aromatic ring in their  
86 structure have been applied for the adsorption of different pollutants, such as phenolic  
87 compounds (Luo et al., 2015), aniline (Gu et al., 2014), bisphenol A (Yang et al., 2016),  
88 naphthalene and phenanthrene (Changchaivong and Khaodhiar, 2009). The mechanism of  
89 interaction involves both  $\pi$ - $\pi$  interactions between aromatic rings of the surfactant and the  
90 rings of the pollutant and other organic interactions (hydrogen bonding, London forces, etc),  
91 making these modified clays better adsorbents (Oliveira et al., 2017; Oliveira and Guégan,  
92 2016). Indeed, hexadecylpyridinium chloride was used, commonly applied as an antibacterial  
93 agent widely in antiseptic solutions and some personal care products, as well as a preservative  
94 in pharmaceutical preparations and in the meat industry as a spray for the control of microbial  
95 growth (Herrera et al., 2004; Özdemir et al., 2013).

96 Furthermore, the adsorption of organic pollutants is improved when the incorporated  
97 amount of surfactant is higher than the cationic exchange capacity (CEC) of the clay mineral  
98 (Brito et al., 2018; Luo et al., 2018).

99 In the present study, organoclays were obtained by the organofunctionalization of  
100 bentonite, a mineral constituted predominantly by  $\geq 50\%$  smectite, most commonly  
101 montmorillonite (Mt). Mt is a 2:1 phyllosilicate with a general structure of  $(M^{x+}, nH_2O)(Al^{3+}_{2-}$   
102  $_yMg^{2+}_ySi^{4+}_4O_{10}(OH)_2$ , where  $Si^{4+}$  ions are coordinated to four oxygens in tetrahedral sites and  
103  $Mg^{2+}/Al^{3+}$  ions are octahedrally coordinated to six oxygens. The hydrated interlayer cations  
104  $M^{x+}$  (commonly  $Na^+$  or  $Ca^{2+}$ ) balance the negative layer charge due to the isomorphic  
105 substitution of  $Mg^{2+}$  for  $Al^{3+}$  in the octahedral sheet. These interlayer cations can be  
106 exchanged by organic cations in water solution, resulting in organophilic bentonite derivatives  
107 (Lagaly et al., 2013).

108 Therefore, in this case, organobentonites were synthesized through microwave (MW)  
109 heating in a very short time (5 min) by reaction with two alkylpyridinium surfactants that  
110 have aromatic rings in their structure. The influences of the chain length and composition of  
111 both molecules on the synthesis of organobentonites, and diclofenac adsorption on modified  
112 clay samples was evaluated. The synthesized samples were used for the first time for  
113 diclofenac adsorption. The tests of drug adsorption were conducted under different  
114 experimental conditions, and the influence of adsorbent dosage, pH, time and initial  
115 diclofenac concentration were investigated. New insights in the mechanism of drug/solid  
116 adsorption were also suggested based on characterization of the adsorbents after drug  
117 adsorption.

## 118 **2. Experimental**

### 119 **2.1 Materials**

120 A sodium bentonite sample (BentNa), CEC 74.64 cmol(+)/kg, was supplied by  
121 Bentonise Bentonita Company, Brazil. The chemical composition of the bentonite was as  
122 follows:  $SiO_2$  (52.98%),  $Al_2O_3$  (18.35%),  $Fe_2O_3$  (3.96%),  $TiO_2$  (0.18%),  $CaO$  (0.01%),  $MgO$

123 (2.47%), Na<sub>2</sub>O (2.56%), K<sub>2</sub>O (0.22%) and fire loss 18.59% (Cavalcanti et al., 2019). 1-  
124 Dodecylpyridinium chloride hydrate (C<sub>12</sub>pyCl) and hexadecylpyridinium chloride  
125 monohydrate (C<sub>16</sub>pyCl) with purity grades of 98% and 99%, respectively, were supplied by  
126 Sigma-Aldrich and used as received. Diclofenac sodium salt (CAS number 15307-79-6, MM  
127 = 318.13 g mol<sup>-1</sup> and pKa 4.1) was purchased from Sigma-Aldrich.

## 128 **2.2 Preparation of the alkylpyridinium bentonites**

129 Organobentonites were synthesized based on a previous procedure (Brito et al., 2018).  
130 Initially, two solutions of the salts were prepared in concentrations corresponding to 100 and  
131 200% of the CEC of the bentonite. A sample of 4.0 g of BentNa was suspended in 100 mL of  
132 each surfactant solution in a Teflon vessel reactor and heated in a microwave reactor (IS-TEC  
133 MW reactor model RMW-1, Brazil, with a power of 1100 W and 2.45 GHz) for 5 min at 50  
134 °C. The obtained solids were recovered by centrifugation at 10000 rpm, washed with distilled  
135 water until testing negative for chlorite with 0.01 mol L<sup>-1</sup> AgNO<sub>3</sub> and dried in an oven for at  
136 least 24 h at 50 °C.

## 137 **2.3 Diclofenac sorption**

138 The test of diclofenac adsorption followed a previous method (Brito et al., 2018;  
139 França et al., 2019), by which the influences of the medium pH (6.0-10.0), dosage of the solid  
140 (25-400 mg), time (0.5 – 120 min) and drug initial concentration (1-500 mg L<sup>-1</sup>) were  
141 evaluated.

142 Batch tests were performed at 30 °C by using samples of organobentonites dispersed  
143 in 20 mL of diclofenac solution. This temperature is the medium temperature found for  
144 Brazilian aquatic bodies. After each test, the solids were recovered by centrifugation, and the  
145 diclofenac concentrations were monitored by UV-Vis molecular spectrometry (Shimadzu

146 spectrometer model TCC-240 240) at 276 nm (Ghemit et al., 2019). The amount of adsorbed  
147 drug ( $q$ ) was calculated as established in Eq. 1:

$$148 \quad q = \frac{(C_i - C_e)V}{m} \quad (1)$$

149  
150 where  $C_i$  and  $C_e$  are the drug concentrations before and after adsorption ( $\text{mg L}^{-1}$ ),  
151 respectively,  $V$  is the total volume of drug solution (L) and  $m$  is the mass of the solid (g).

152 To investigate pH, 50 mg of solids was reacted with 20 mL of  $100 \text{ mg L}^{-1}$  diclofenac  
153 solution for 24 h. The pH was adjusted with  $0.05 \text{ mol L}^{-1}$  NaOH or  $\text{HNO}_3$  solutions.

154 Tests for the dosage of solids were monitored at optimum pH under the same  
155 conditions described.

156 Tests for different times of interaction were conducted with the fixed mass obtained in  
157 the solid dosage tests and at optimum pH for times in the range of 0.5-120 min.

158 Finally, the initial diclofenac concentrations were evaluated in the range of 1-500 mg  
159  $\text{L}^{-1}$  at the optimized pH, dosage of solids and time of contact.

160 All experiments were performed in triplicate.

## 161 **2.4 Kinetic and equilibrium models**

162 The experimental data were adjusted to fit the following kinetic models: pseudo-first-  
163 order (Lagergren, 1898), pseudo-second-order (Ho and McKay, 1999) and simplified Elovich  
164 equation (Chien and Clayton, 1984), assuming  $\alpha\beta t \gg 1$ , (see Eqs. 1 to 3 in Supplementary  
165 Material SII).

166 The equilibrium isotherms were analyzed with the Langmuir (Langmuir, 1918),  
167 Freundlich (Freundlich, 1906) and Temkin (Temkin and Pyzhev, 1940) models (see Eqs. 4-6  
168 in Supplementary Material SII).



169 The standard deviation (SD-root mean square error), Eq. 2, was used to verify which  
170 equation models were best suited to describe the experimental data (Lima et al., 2015).

171

$$172 \quad SD = \sqrt{\frac{1}{n_p - p} \sum_i^n (q_{i,exp} - q_{i,model})^2} \quad (2)$$

173

174 where  $q_{i,exp}$  and  $q_{i,model}$  are the experimental adsorbed drug amount and theoretical  
175 amount obtained by the kinetic models,  $n_p$  is the number of performed experiments, and  $p$  is  
176 the number of parameters of the fitted model.

## 177 2.5 Characterizations

178 X-ray diffraction (XRD) analyses were conducted on a Shimadzu XD3A model  
179 diffractometer with  $CuK\alpha$  radiation and a fixed power source (40 kV and 30 mA). FTIR  
180 spectra were recorded in the 4000-400  $cm^{-1}$  region by a Shimadzu IR Prestige-21 model; the  
181 samples were dispersed in KBr pellets, and a resolution of 4  $cm^{-1}$  and accumulation of 20  
182 scans were used for each run. Thermogravimetry data for the solids were obtained using an  
183 SDT Q600 V20.9 Build 20 thermal analyzer with a heating rate of 10  $^{\circ}C \text{ min}^{-1}$  under 100 mL  
184  $min^{-1}$  of argon flow in the range of 30 to 900  $^{\circ}C$ . CHN elemental analysis was obtained by  
185 using a Perkin-Elmer PE-2400 microelemental analyzer. Chloride was analyzed by titration:  
186 samples of 100 mg in triplicate was suspended in 0.01  $mol \text{ L}^{-1}$   $NaNO_3$  for 24 h at 25  $^{\circ}C$ . The  
187 dispersions were centrifuged and the procedure was repeated 3 times to ensure the exchange  
188 of  $Cl^-$  by  $NO_3^-$ . After centrifugation, aliquots of 10 mL of supernatant were titrated with  
189 standard  $AgNO_3$  solution (Skoog et al., 2012). Zeta potential ( $\zeta$ ) was measured using a  
190 Zetasizer Nano Zs (Malvern Instruments) for isoelectric titration through pH titration. The pH  
191 of the solutions was adjusted with 0.100  $mol \text{ L}^{-1}$   $NaOH$  or 0.500  $mol \text{ L}^{-1}$   $HNO_3$ .

## 192 3. Results and discussion

### 193 3.1 X-ray diffraction

194

195 The XRD pattern of BentNa (Figure SM1a) showed smectite with sodium  
196 montmorillonite (Mt) as the predominant phase and impurities of quartz (Q) and muscovite  
197 (M), in agreement with ICDD cards 00.029.1498, 00.058.2036 and 01.070.8055 and previous  
198 studies (Cavalcanti et al., 2019; Queiroga et al., 2019). Characteristic reflections of Mt at  $2\theta =$   
199  $7.37^\circ$  suggested a basal spacing ( $d_{001}$ ) of 1.12 nm, as further indicated by additional  
200 reflections at  $2\theta$  values of  $19.6^\circ$ ,  $28.3^\circ$ ,  $35.0^\circ$  and  $61.8^\circ$ .

201 The intercalation of alkylpyridinium cations was confirmed by the increase in basal  
202 spacings to 1.56, 1.74, 1.66 and 2.13 nm for Bent-C<sub>12</sub>py-100%, Bent-C<sub>16</sub>py-100%, Bent-  
203 C<sub>12</sub>py-200% and Bent-C<sub>16</sub>py-200% (Figure SM1), respectively. The results indicated that  
204 higher values were observed for solids prepared with 200% of the CEC and a longer organic  
205 chain of the salt (Changchaivong and Khaodhiar, 2009; Greenland and Quirk, 1962; Muñoz-  
206 Shugulí et al., 2019).

207 Studies have established that the size of the organic chain and the intercalated amount  
208 determine the arrangement of surfactants in the interlayer spacing. For example, C<sub>16</sub>py<sup>+</sup>  
209 monolayer ( $d_{001} = 1.32\sim 1.47$  nm), bilayer ( $d_{001} = 1.68\sim 1.78$  nm) and pseudotrilayer ( $d_{001} =$   
210  $2.14\sim 2.20$  nm) arrangements in the gallery spacing of montmorillonite have been proposed  
211 (Meleshyn and Bunnenberg, 2006). Based on the size of the surfactant molecules and the final  
212 basal spacings (Chen et al., 2005; Luo et al., 2018), monolayer arrangement occurred for  
213 Bent-C<sub>12</sub>py-100%, bilayer arrangement occurred for Bent-C<sub>12</sub>py-200% and Bent-C<sub>16</sub>py-  
214 100%, and pseudotrilayer arrangement occurred for Bent-C<sub>16</sub>py-200%, as illustrated in Figure  
215 SM2.

216 The XRD results were compared with previous studies that considered the synthesis of  
217 organobentonites by using conventional and microwave heating with the same proportion of  
218 surfactant adopted in the present work (Table SM1). The obtained values for Bent-C<sub>16</sub>py are  
219 close to those obtained by (Schampera and Dultz, 2009) and Muñoz-Shugulí et al. (2019)  
220 using conventional heating at times of 20 and 1 h at 60 °C, respectively. However, divergent  
221 values were also observed and were associated with the different CECs of the pristine  
222 bentonites used (He et al., 2014) different conditions of synthesis. Therefore, the studies  
223 showed that aspects such as washing and drying (Luo et al., 2016) and the nature of the  
224 interlayer cations (Volzone et al., 2002) can influence the final basal spacing and the amount  
225 of intercalated surfactant.

226

### 227 **3.2 CHNCl elemental analysis**

228

229 The amount of incorporated surfactant in the bentonite was determined based on C and  
230 N elemental analysis (Table 1); the values were close to the CEC (~ 90% of the initial salt  
231 concentration) for Bent-C<sub>12</sub>py-100% and Bent-C<sub>16</sub>py-100% and were near that for  
232 montmorillonites modified with C<sub>16</sub>py<sup>+</sup> using 100% of the CEC by conventional heating  
233 (Schampera and Dultz, 2009).

234 For the organobentonites obtained using 200% of the CEC of BentNa, only Bent-  
235 C<sub>16</sub>py-200% exhibited a value higher than the CEC (112.4%), while C<sub>12</sub>py-200% exhibited a  
236 value of 93.3%. The excess of surfactant in Bent-C<sub>16</sub>py-200% was incorporated as the ion  
237 pair C<sub>16</sub>pyCl through hydrophobic interactions between the alkyl tails of the organic chain  
238 (Luo et al., 2018; Meleshyn and Bunnenberg, 2006), and was further verified by the presence  
239 of the chloride in the organoclays (Table 1). No Cl<sup>-</sup> ions were detected in other  
240 organobentonites (Bent-C<sub>12</sub>py-100%, Bent-C<sub>16</sub>py-100% and Bent-C<sub>12</sub>py-200%).

241 The better affinity of bentonite for surfactants with longer organic chains was related  
242 to an increase in the contribution of Van der Waals interactions and a decrease in the  
243 hydration enthalpy of the organic salt, favoring intercalation (Teppen and Aggarwal, 2007).

244 This result suggested that the packing densities of the groups in the solids can be  
245 influenced by the amount of intercalated molecules.

246

### 247 **3.3 Infrared spectroscopy**

248

249 Infrared spectra were used to monitor the organofunctionalization of the bentonite;  
250 therefore, the spectra of the pristine and modified solids are shown in Figure SM3. For  
251 sodium bentonite, typical bands were detected at  $3632\text{ cm}^{-1}$  and  $3440\text{ cm}^{-1}$ , assigned to the  
252 hydroxyl stretching of structural M-OH ( $M = \text{Al}^{3+}$ ,  $\text{Mg}^{2+}$  or  $\text{Fe}^{3+}$ ) and silanol. The bending of  
253 water molecules was also observed at  $1638\text{ cm}^{-1}$  (Slaný et al., 2019).

254 For the region below  $1200\text{ cm}^{-1}$ , bands at  $1115$  and  $1042\text{ cm}^{-1}$  were related to Si-O  
255 stretching, and bands at  $915\text{-}847\text{ cm}^{-1}$  were due to AlMOH deformation ( $M = \text{Al}$ ,  $\text{Fe}$  or  $\text{Mg}$ )  
256 (Slaný et al., 2019). The presence of quartz impurities was confirmed by the Si-O deformation  
257 at  $798\text{ cm}^{-1}$ . Other bands at  $620$ ,  $519$  and  $465\text{ cm}^{-1}$  were assigned to Al-O/Si-O, Al-O-Si and  
258 Si-O-Si deformations, respectively, and are characteristic of montmorillonite (Slaný et al.,  
259 2019).

260 The intercalation of the surfactants in the clay minerals was accompanied by the  
261 appearance of new bands in the range of  $3136\text{-}3096\text{ cm}^{-1}$ , attributed to the aromatic CH  
262 stretching of pyridine rings, and from  $2928\text{-}2851\text{ cm}^{-1}$ , related to  $\text{CH}_2$  antisymmetric and  
263 symmetrical stretching vibrations (Lin-Vien et al., 1991; Luo et al., 2018). The location of the  
264  $\nu_{\text{as}}(\text{CH}_2)$  band at wavelengths higher than those of free surfactants (Table SM2) suggests the

265 existence of structures with a disordered arrangement of organic cations (gauche conformers)  
266 in the interlayer region of the montmorillonite (Chen et al., 2005; Slaný et al., 2019).

267 The spectra also exhibited a low-intensity band at 1502  $\text{cm}^{-1}$  associated with C=C  
268 vibrations of aromatic rings, bands at 1486 and 1469  $\text{cm}^{-1}$ , associated with  $\text{CH}_3$  and  $\text{CH}_2$   
269 deformations, respectively and a band at 729  $\text{cm}^{-1}$ , related to  $(\text{CH}_2)_n$  in-phase rocking,  
270 characteristic of alkyl chains of surfactants (Lin-Vien et al., 1991; Slaný et al., 2019). The  
271 absorptions at 777 and 679  $\text{cm}^{-1}$  were assigned to deformation of the pyridine ring (Lin-Vien  
272 et al., 1991).

### 273 **3.4 Thermogravimetry**

274

275 Thermogravimetry is a useful tool to quantify the amount of organic content in a solid  
276 but is also associated with other techniques, such as XRD and FTIR, to characterize how  
277 surfactants are confined in the interlayer region (Chen et al., 2005). TG curves (Figure SM4)  
278 and the associated mass losses are summarized in Table SM3.

279 The TG curve of pristine bentonite exhibited two steps of mass loss, the first step at  
280 30-200  $^{\circ}\text{C}$ , attributed to the elimination of the interlayer water and water adsorbed on the  
281 surface, and the second from 200-900  $^{\circ}\text{C}$ , associated with the condensation of structural OH  
282 (Muñoz-Shugulí et al., 2019).

283 The organobentonites showed four and five events of mass loss. For all samples, the  
284 first event associated with the elimination of water was  $\leq 1.2\%$ , suggesting the hydrophobic  
285 nature of the organoclays (Muñoz-Shugulí et al., 2019). Additionally, the sum of mass losses  
286 of the other events was higher than in the pristine clay and are associated to an exothermal  
287 event (Heat flow not presented), which was an indication of the presence of organic moieties  
288 in the solids.

289 The initial temperature associated with the degradation of the organic part decreased  
290 as the incorporated amount of surfactant increased and was observed at 182, 175, 174 and 118  
291 °C for the Bent-C12py-100%, Bent-C16py-100% Bent-C12py-200% and Bent-C16py-200%  
292 solids, respectively; this degradation finished at 513-520 °C; therefore, the number of  
293 decomposition events exhibited within this range depended on the types of interactions (Chen  
294 et al., 2005; Muñoz-Shugulí et al., 2019).

295 Meleshyn and Bunnenberg, (2006) suggested that a lower temperature for the exit of  
296 surfactants occurs due to the different arrangements of organic chains in the interlayer spacing  
297 of clay samples and is an indication of weaker interactions (lower energy) between the  
298 organic cations and the mineral surface. In other words, as the organic cation content  
299 increases, the configurations change from monolayer and bilayer to pseudotriloader, in  
300 accordance with the observed results.

301 Above 520 °C, mass loss was attributed to dehydroxylation (Luo et al., 2018; Muñoz-  
302 Shugulí et al., 2019).

303

### 304 **3.5 Zeta potential**

305

306 Zeta potential measurements (Figure SM5) suggested that the point of zero charge  
307 ( $\text{pH}_{\text{PZC}}$ ) occurred at pH 3.4, 2.5, 4.1 and 8.1 for Bent-C<sub>12</sub>-100%, Bent-C<sub>16</sub>-100%, Bent-C<sub>12</sub>-  
308 200% and Bent-C<sub>16</sub>-200%, respectively. BentNa is negatively charged in all pH ranges. The  
309 modification of clay minerals with cationic surfactants promotes a total or partial variation in  
310 surface charge, depending on the amount of organic cations incorporated (Brito et al., 2018;  
311 Schampera and Dultz, 2009). Therefore, the values of  $\text{pH}_{\text{PZC}}$  observed for Bent-C<sub>12</sub>-100%,  
312 Bent-C<sub>16</sub>-100% and Bent-C<sub>12</sub>-200% are probably related to the low amount of surfactant  
313 incorporated (~ 90% of the CEC), while the higher value of  $\text{pH}_{\text{PZC}}$  for Bent-C<sub>16</sub>-200% is

314 consistent with the excess surfactant adsorbed probably on the basal surface of the bentonite  
315 sample, as indicated by the CHNCl and thermogravimetry results.

316

### 317 **3.7 Adsorption of diclofenac on the solids**

#### 318 **3.7.1 Influence of pH**

319 The effect of pH on the adsorption process has often been evaluated according to the  
320 different behaviors presented by drugs and solids in aqueous media (Ghemit et al., 2019;  
321 Oliveira et al., 2017). This parameter was analyzed considering the speciation of the  
322 diclofenac molecule at different pH values (Figure SM6i) and zeta potential measurements ( $\zeta$ )  
323 (Figure SM5). The results showed that the adsorption depended slightly on the pH (Figure  
324 SM6ii); the maximum values were 12.87, 18.19, 25.30 and 39.40 mg g<sup>-1</sup> for Bent-C<sub>12</sub>-100%,  
325 Bent-C<sub>16</sub>-100%, Bent-C<sub>12</sub>-200% and Bent-C<sub>16</sub>-200%, respectively, at pH 6.0 and were better  
326 than those at pH 8 and 10.

327 Based on the pKa (4.1) of diclofenac, at pH  $\geq$  6, the anionic form dominates, and the  
328 decreased adsorption with increased pH (6-10) for Bent-C<sub>12</sub>-100%, Bent-C<sub>16</sub>-100% and Bent-  
329 C<sub>12</sub>-200% can be associated with the repulsion between deprotonated diclofenac and  
330 organobentonites (Luo et al., 2015), considering the pH<sub>PZC</sub> value; at pH < pH<sub>PZC</sub>, the surface  
331 is positively charged, and the surface is negatively charged for pH values above the pH<sub>PZC</sub>.  
332 These results suggested that non-electrostatic interactions contributed to the mechanism of  
333 adsorption.

334

#### 335 **3.7.2 Dosage of the adsorbent**

336 The dosage of the adsorbent (Figure SM7) is important for establishing the best  
337 adsorption efficiency of the drug from solution. The adsorption percentages increase

338 gradually with increased organobentonite mass due to the increase of interaction sites amount  
339 (Brito et al., 2018; Ghemit et al., 2019).

340 The best performance was observed for 300, 200, 150 and 50 mg of Bent-C<sub>12</sub>-100%,  
341 Bent-C<sub>16</sub>-100%, Bent-C<sub>12</sub>-200% and Bent-C<sub>16</sub>-200%, respectively and these dosages were  
342 associated with adsorption efficiencies of 88.3, 97.1, 93.5 and 99.5%. The adsorbed amounts  
343 per gram of adsorbent (q) were 5.9 mg g<sup>-1</sup> for Bent-C<sub>12</sub>py-100%, 9.3 mg g<sup>-1</sup> for Bent-C<sub>16</sub>py-  
344 100%, 13.0 mg g<sup>-1</sup> for Bent-C<sub>12</sub>py-200% and 38.7 mg g<sup>-1</sup> para Bent-C<sub>16</sub>py-200% (Figure  
345 SM7ii).

346

### 347 **3.7.3 Kinetic studies**

348 Adsorption kinetic studies of diclofenac (Figure SM8) were carried out using the  
349 masses corresponding to the maximum percentages of diclofenac adsorption obtained in the  
350 evaluation of the adsorbent dosage effect at pH 6.0. The isotherms showed rapid adsorption of  
351 the drug by the organophilic clays at 60 and 10 min for the solids obtained with 100% and  
352 200% of the CEC, respectively. These results were close to those observed for other  
353 organophilic clays used for diclofenac adsorption (Ghemit et al., 2019; Sun et al., 2017a).

354 The adsorption kinetics were analyzed by nonlinear regression of the isotherms to the  
355 pseudo-first-order, pseudo-second-order and Elovich models, whose parameters are  
356 summarized in Table 2. In addition to R<sup>2</sup>, the fit of the isotherms to the models was also  
357 evaluated using the standard deviation (SD) (Lima et al., 2015), which showed a better fit to  
358 the Elovich equation for Bent-C<sub>12</sub>py-100% and Bent-C<sub>16</sub>py-100% and a better fit to the  
359 pseudo-second-order model for Bent-C<sub>12</sub>py-200% and Bent-C<sub>16</sub>py-200%. The Elovich model  
360 describes the process as chemisorption and considers the heterogeneity of the surface of the  
361 adsorbent (Lima et al., 2015).

362



### 363 3.7.4 Adsorption isotherms

364 The equilibrium isotherms were evaluated at 1-500 mg L<sup>-1</sup> diclofenac (Figure 1), pH 6  
365 and 60 min. The isotherms for the organobentonites initially showed an increase in adsorbed  
366 amount ( $q_e$ ) with increased drug concentration, reaching almost constant values at initial  
367 concentrations ( $C_i$ ) of 350 mg L<sup>-1</sup> for Bent-C<sub>16</sub>py-100% and Bent-C<sub>12</sub>py-200%, 300 mg L<sup>-1</sup>  
368 for Bent-C<sub>16</sub>py-200% and 450 mg L<sup>-1</sup> for Bent-C<sub>12</sub>py-100%.

369 The maximum adsorption capacities ( $q_{max}$ ) were 13.02, 19.30, 25.50 and 91.13 mg g<sup>-1</sup>  
370 on Bent-C<sub>12</sub>py-100%, Bent-C<sub>16</sub>py-100%, Bent-C<sub>12</sub>py-200% and Bent-C<sub>16</sub>py-200%,  
371 respectively. The result for pristine bentonite was less than 5% of the reported values (< 5 mg  
372 g<sup>-1</sup>) under the same conditions. These results were also compared with the diclofenac  
373 adsorption capacity on other organoclays samples obtained from conventional procedure at  
374 time of 15-72 h (Table SM4), and illustrated the good performance of the organobentonites  
375 obtained in this study in only 5 min by microwave irradiation. Long time reactions is a  
376 limitation for use of organoclays industrial scale (Yapar, 2009), however, the use of  
377 microwave irradiation behaved as good alternative for rapid and reproductive preparation of  
378 modified clay minerals.

379 Beyond the low-cost and good efficiency of the organobentonites, the choice of  
380 adsorbent depends of other factors such biocompatibility with the ecosystem and their  
381 regeneration and recycle (Biswas et al., 2019; Momina et al., 2018), that were not studied in this  
382 present case.

383 Some organoclays exhibited high toxicity (Sarkar et al., 2013; Witthuhn et al., 2005) while  
384 others did not showed any toxicity for the original community of soil microorganisms responsible  
385 for biodegradation (Abbate et al., 2013), therefore, the toxicity of alkyipyridium bentonites remains  
386 still unknown. The antibacterial activities of hexadecylpyridinium-montmorillonites was verified  
387 only against some bacteria responsible for infections in humans and animals and food

388 contamination (Herrera et al., 2000; Malachová et al., 2009; Özdemir et al., 2013), and when  
389 added to the diet of weaned pigs was proposed as an alternative to antibiotic chlortetracycline  
390 for improving growth performance, mucosal architecture and modifying intestinal microflora  
391 (Ke et al., 2014). Moreover, some studies observed that these solids can be used as precursor  
392 to obtain new materials such as porous clay heterostructures (Zhu et al., 2005) or carbon-clay  
393 composites (Jović-Jovičić et al., 2019).

394 Comparing the results for solids modified with the same surfactant, better adsorption  
395 was observed for adsorbents with a higher organic content and basal spacing, for example  
396 organobentonite prepared with 100 and 200% of the CEC. Similar results were observed in  
397 previous studies for organobentonites prepared with hexadecyltrimethylammonium (Ghemit  
398 et al., 2019; Sun et al., 2017a).

399 In addition, the nature of the surfactant, packing density, amount incorporated and  
400 organization of the organic cations in the interlayer region can influence drug adsorption in  
401 aqueous media (Oliveira et al., 2017; Oliveira and Guégan, 2016). Organic pollutant  
402 adsorption on organophilic pyridinium montmorillonites is dependent on these cited effects  
403 (Chen et al., 2005; Gu et al., 2014; Luo et al., 2015), as has also been observed for inorganic  
404 pollutants (Luo et al., 2017). The cited studies demonstrate that the different characteristics of  
405 organoclays influence their affinity for pollutants and, in some cases, their interaction  
406 mechanisms.

407 In this present case, the obtained  $q_e$  values for diclofenac adsorption on Bent-C<sub>12</sub>py-  
408 100%, Bent-C<sub>16</sub>py-100% and Bent-C<sub>12</sub>py-100% were also influenced by the packing density  
409 and the organization of alkylpyridinium cations inside the interlayer spacing since these  
410 adsorbents presented lower amounts of incorporated surfactants (close to the CEC) but  
411 different  $d_{001}$  and cation sizes.

412 The data were evaluated according to the Langmuir, Freundlich and Temkin  
413 adsorption models, and the parameters obtained are summarized in Table 3. From the values  
414 of  $R^2$  and SD, the experimental data were better fit by the Langmuir model for all  
415 organobentonitas, indicating that chemisorption can be the preponderant mechanism involved  
416 in the diclofenac adsorption. Langmuir model is based on the existence of homogenous  
417 adsorption sites. The adjustment was better for Bent-C<sub>12</sub>py-100% sample (higher  $R^2$  and  
418 lower SD), which is an indication of more uniformed distribution of the adsorptions sites of  
419 the same nature.

420

### 421 **3.7.5 Characterization of the drug/clay mineral hybrids**

#### 422 **3.7.5.1 X-ray diffraction**

423 XRD patterns of the drug/clay mineral hybrids (Figure 2) obtained with 10, 100 and  
424 500 mg L<sup>-1</sup> of initial drug concentrations did not present alterations in the basal spacing, as  
425 observed in the literature for organophilic montmorillonites (Oliveira et al., 2017; Oliveira  
426 and Guégan, 2016; Sun et al., 2017a).

427 The adsorption of a drug in the interlayer region of a clay mineral can drive the  
428 rearrangement of the surfactant molecules without changes in the value of the basal spacing  
429 (Meleshyn and Bunnenberg, 2006; Oliveira et al., 2017; Oliveira and Guégan, 2016; Sun et  
430 al., 2017a). For the sample Bent-C<sub>12</sub>py-200% ( $d_{001} = 1.66$  nm), the packaging density was  
431 higher than that for Bent-C<sub>12</sub>py-100% ( $d_{001} = 1.56$  nm). Consequently, the entrance of the  
432 drug would be more difficult for Bent-C<sub>12</sub>py-200%, however the adsorption was higher for  
433 this sample. It more reasonable that the drug did not access more internal adsorption sites.

434 For Bent-C<sub>16</sub>py-200%, the behavior was different once the basal spacing was 2.13 nm,  
435 the amount of organic salt in the solid was higher than the CEC (0.84 mmol g<sup>-1</sup>) associated

436 with the presence of the C<sub>16</sub>pyCl ionic pair. Therefore, the presence of chloride in the  
437 equilibrium solution after drug adsorption was a strong indication of another mechanism for  
438 adsorption, such as anion exchange between the Cl<sup>-</sup> ions and anionic drug. Similar results  
439 have also been described previously in perchlorate adsorption (Chitrakar et al., 2012; Luo et  
440 al., 2016). The literature shows that Cl<sup>-</sup> ions in C<sub>16</sub>py<sup>+</sup>-modified montmorillonite were located  
441 near the mid plane of the interlayer space (Meleshyn and Bunnenberg, 2006) and are therefore  
442 accessible adsorption sites for anionic species, such as diclofenac.

443

### 444 **3.7.5.2 Infrared spectroscopy**

445

446 For better analysis of the results, the infrared spectra of the free drug and drug/solid  
447 hybrids prepared at 10, 100 and 500 mg L<sup>-1</sup> diclofenac were divided into three regions,  
448 (Figures 3 and SM9). Therefore, infrared spectra in the region of 4000-2750 cm<sup>-1</sup> showed  
449 diclofenac bands at 3388 and 2357 cm<sup>-1</sup> assigned to free and bound N-H stretching,  
450 respectively, the latter through intramolecular hydrogen bonds (N-H<sup>⋯</sup>O) (Kovala-Demertzi et  
451 al., 1993; Lin-Vien et al., 1991). The bands at 3080 and 3036 cm<sup>-1</sup> were attributed to  $\nu(\text{C-}$   
452  $\text{H})_{\text{aromatic}}$ , and those at 2971 and 2897 cm<sup>-1</sup> were due antisymmetric and symmetric aliphatic  
453 CH<sub>2</sub> stretching (Lin-Vien et al., 1991). For the drug/Bent-C<sub>16</sub>-200% hybrid, the initial band of  
454 OH stretching of water at 3410 cm<sup>-1</sup> was shifted to 3430-3422 cm<sup>-1</sup> for solids with 3.71 mg g<sup>-1</sup>  
455 (C<sub>i</sub> = 10 mg L<sup>-1</sup>) and 91.13 mg g<sup>-1</sup> (C<sub>i</sub> = 500 mg L<sup>-1</sup>). For the other solids with diclofenac, no  
456 alteration was observed in this region.

457 For region 2 (1750-1250 cm<sup>-1</sup>), diclofenac presents typical bands associated with  
458 aromatic ring stretching at 1603 and 1556 cm<sup>-1</sup>, a band at 1507 and 1500 cm<sup>-1</sup> assigned to C-  
459 N-H bending of the secondary amine and C-H rock of aromatic rings, band at 1468 cm<sup>-1</sup> due  
460 to C-N stretching and C-H rock (aromatic ring), and bands at 1452 and 1305 cm<sup>-1</sup> attributed to

461 CH<sub>2</sub> bending (Iliescu et al., 2004; Lin-Vien et al., 1991). The samples with adsorbed  
462 diclofenac showed broader bands of aromatic ring stretching at 1558 cm<sup>-1</sup> and CH<sub>2</sub> bending at  
463 1455 cm<sup>-1</sup>.

464 The diclofenac infrared spectrum also presents bands at 1575 and 1400 cm<sup>-1</sup>, assigned  
465 to antisymmetric and symmetrical stretching of carboxylate group, respectively. The observed  
466 wavenumber variation  $\Delta\nu(\text{COO}^-)$  of 175 cm<sup>-1</sup> is characteristic of the drug in ionic form  
467 (Kovala-Demertzi et al., 1993). Therefore, both bands were detected at 1580~1584 cm<sup>-1</sup> and  
468 1378~1370 cm<sup>-1</sup> for all organobentonite/drug solid samples, suggesting that -COO<sup>-</sup> groups  
469 were also involved, possibly through electrostatic interaction (Sun et al., 2017b, 2017c).

470 The occurrence of electrostatic interactions between diclofenac and Bent-C<sub>12</sub>-100%,  
471 Bent-C<sub>16</sub>-100% and Bent-C<sub>12</sub>-200% is not probable due to the negative charges of the  
472 surfaces at pH 6.0. Similar behavior was observed for an organophilic montmorillonite  
473 obtained using a concentration of C<sub>16</sub>pyCl at 92% of the CEC (Luo et al., 2017). Although the  
474 surface was negatively charged and the amount was lower than the CEC, ReO<sub>4</sub><sup>-</sup> was adsorbed.  
475 The proposed interaction was associated with the desorption of the surfactant weakly bound  
476 to montmorillonite, capturing of anions in solution and subsequent adsorption of C<sub>16</sub>py<sup>+</sup>ReO<sub>4</sub><sup>-</sup>  
477 on the external surface by hydrophobic interactions. This same mechanism was also  
478 suggested for the adsorption of ClO<sub>4</sub><sup>-</sup> anions on C<sub>16</sub>py<sup>+</sup>.montmorillonite (Luo et al., 2016).

479 Finally, region 3 of the FTIR spectrum for free diclofenac presented bands at 766, 746  
480 and 714 cm<sup>-1</sup> assigned to C-H deformation (Kovala-Demertzi et al., 1993) and characteristic  
481 of 1,2-disubstituted and 1,2,3-trisubstituted aromatic rings (Iliescu et al., 2004), and the band  
482 at 635 cm<sup>-1</sup> is characteristic of ring deformation modes (Lin-Vien et al., 1991). For this  
483 region, only Bent-C<sub>16</sub>-200% exhibited a shoulder at 746 cm<sup>-1</sup> when a high initial drug  
484 concentration was used.

485

### 486 3.7.6 Mechanism of drug interaction

487 The new properties of the organophilic clays were attributed to a change in character  
488 from hydrophilic to hydrophobic, anion exchange as a consequence of the incorporation of  
489 excess surfactant and different packing densities and arrangements of the organic cations in  
490 the interlayer region, which favor interactions with pollutants (Oliveira et al., 2017; Oliveira  
491 and Guégan, 2016). Thus, the different characteristics presented by each solid contributed in  
492 several forms to diclofenac adsorption due to the different affinities, as observed in the values  
493 of  $q_{\max}$ .

494 A theoretical study realized by Meleshyn and Bunnenberg (2006) indicated that  
495 interlayer anion sorption on montmorillonite modified with  $C_{16}pyCl$  occurs only for higher  
496 surfactant contents and basal spacings (2.1~2.2 nm) and consequently when a  
497 pseudotrimolecular form is obtained. In this condition, chloride can be accommodated  
498 between the layers as a counter ion of  $C_{16}py^+$  or sodium cations. Several works have shown  
499 that some of the interlayer cations of pristine bentonite remain in the bentonite structure even  
500 when the amount of  $C_{16}py^+$  incorporated is equal to or higher than the CEC and act as cation  
501 or anion exchange sites (Chitrakar et al., 2012; Luo et al., 2016), in agreement with the  
502 theoretical study (Meleshyn and Bunnenberg, 2006).

503 Based on the CHNCl results, the amount of surfactant higher than the CEC and the  
504 presence of chloride ions ( $0.154 \text{ mmol g}^{-1}$ ) were observed only for Bent- $C_{16}py$ -200%. In this  
505 case,  $0.145 \text{ mmol g}^{-1} Cl^-$  was detected in the equilibrium solution after diclofenac adsorption,  
506 which was half of the maximum diclofenac adsorbed ( $0.291 \text{ mmol g}^{-1}$ ).

507 For the other solids, although the amount of alkylpyridinium cation incorporated was  
508 lower than the CEC of the pristine bentonite, the FTIR results also suggested electrostatic  
509 between the incorporated surfactant (pyridinium) and the carboxylate groups of diclofenac.

510           However, the influence of the pH on drug adsorption is not electrostatic in nature and  
511           contributes to organophilic (alkyl groups of the salt and ring of the drug) and  $\pi$ - $\pi$  interactions,  
512           the latter between the pyridine rings and the aromatic rings of the pollutant. In particular,  
513           interactions involving  $\pi$  electrons have often been described in the adsorption of aromatic  
514           compounds by pyridinium organophilic clays (Changchaivong and Khaodhiar, 2009; Gu et  
515           al., 2014; Luo et al., 2015; Yang et al., 2016), and for diclofenac adsorption by  
516           benzyltrimethyltetradecylammonium-montmorillonite (Oliveira et al., 2017; Oliveira and  
517           Guégan, 2016). A general scheme of the proposed interaction mechanisms of drug adsorption  
518           on organobentonites was based on obtained results and also in the literature. Depending of the  
519           sample, at least four different contributions were involved in the diclofenac adsorption as  
520           illustrated in Figure 4.

#### 521   **4. Conclusion**

522           The organic modification of bentonite with alkylpyridinium cations through  
523           microwave heating resulted in organophilic clays with different characteristics, which were  
524           dependent on the amount of surfactant and the size of the organic chain, as shown in the CHN  
525           and XRD results. The use of microwave for organophilization of bentonites with both  
526           surfactants at time of 5 min at 50 °C was a promising technique.

527           As a consequence, the organobentonites exhibited different diclofenac adsorption  
528           capacity from aqueous solution, which were probably influenced by the amount of  
529           incorporated surfactant, the packing density and different arrangements of the organic  
530           moieties in the interlayer region. The differences between these factors determine the degree  
531           of affinity of the hybrids for the anionic drug on the surface due to the different adsorption  
532           sites.

533 The drug/organoclay interaction consisted of electrostatic, organophilic and, possibly,  
534  $\pi$ - $\pi$  interactions for all functionalized bentonites. The best performance for diclofenac  
535 adsorption was 91.13 mg g<sup>-1</sup> for Bent-C<sub>16</sub>py-200% due to the excess of surfactant  
536 incorporated. This present study demonstrated the versatility of these solids for anionic  
537 species or even neutral species, considering the presence of different interaction sites.

538

### 539 **Acknowledgement**

540 CNPq is acknowledged for financial support in the form of research fellowships  
541 awarded to M.G. Fonseca (grants 310921-2017-1 and 431727/2016-3) and D.B França  
542 (140661/2017-4). Prof Dalva L.A. Farias (IQ/USP) for her kindly help in Raman  
543 spectroscopy.

### 544 **References**

- 545 Abbate, C., Ambrosoli, R., Minati, J.L., Gennari, M., Arena, M., 2013. Metabolic and  
546 molecular methods to evaluate the organoclay effects on a bacterial community. *Environ.*  
547 *Pollut.* 179, 39–44. <https://doi.org/10.1016/j.envpol.2013.04.012>
- 548 Acuña, V., Ginebreda, A., Mor, J.R., Petrovic, M., Sabater, S., Sumpter, J., Barceló, D., 2015.  
549 Balancing the health benefits and environmental risks of pharmaceuticals: Diclofenac as  
550 an example. *Environ. Int.* 85, 327–333. <https://doi.org/10.1016/j.envint.2015.09.023>
- 551 Andrew Lin, K.-Y., Yang, H., Lee, W.-D., 2015. Enhanced removal of diclofenac from water  
552 using a zeolitic imidazole framework functionalized with cetyltrimethylammonium  
553 bromide (CTAB). *RSC Adv.* 5, 81330–81340. <https://doi.org/10.1039/C5RA08189K>
- 554 Beltrán, F.J., Pocostales, P., Alvarez, P., Oropesa, A., 2009. Diclofenac removal from water  
555 with ozone and activated carbon. *J. Hazard. Mater.* 163, 768–776.  
556 <https://doi.org/10.1016/J.JHAZMAT.2008.07.033>
- 557 Biel-Maeso, M., Baena-Nogueras, R.M., Corada-Fernández, C., Lara-Martín, P.A., 2018.  
558 Occurrence, distribution and environmental risk of pharmaceutically active compounds  
559 (PhACs) in coastal and ocean waters from the Gulf of Cadiz (SW Spain). *Sci. Total*  
560 *Environ.* 612, 649–659. <https://doi.org/10.1016/J.SCITOTENV.2017.08.279>
- 561 Biswas, B., Warr, L.N., Hilder, E.F., Goswami, N., Rahman, M.M., Churchman, J.G.,  
562 Vasilev, K., Pan, G., Naidu, R., 2019. Biocompatible functionalisation of nanoclays for  
563 improved environmental remediation. *Chem. Soc. Rev.* 48, 3740–3770.  
564 <https://doi.org/10.1039/C8CS01019F>



- 565 Bonnefille, B., Gomez, E., Courant, F., Escande, A., Fenet, H., 2018. Diclofenac in the  
566 marine environment: A review of its occurrence and effects. *Mar. Pollut. Bull.* 131, 496–  
567 506. <https://doi.org/10.1016/j.marpolbul.2018.04.053>
- 568 Brito, D.F., Silva Filho, E.C., Fonseca, M.G., Jaber, M., 2018. Organophilic bentonites  
569 obtained by microwave heating as adsorbents for anionic dyes. *J. Environ. Chem. Eng.* 6,  
570 7080–7090. <https://doi.org/10.1016/j.jece.2018.11.006>
- 571 Carballa, M., Omil, F., Lema, J.M., 2005. Removal of cosmetic ingredients and  
572 pharmaceuticals in sewage primary treatment. *Water Res.* 39, 4790–4796.  
573 <https://doi.org/10.1016/J.WATRES.2005.09.018>
- 574 Cavalcanti, G.R.S., Fonseca, M.G., da Silva Filho, E.C., Jaber, M., 2019.  
575 Thiabendazole/bentonites hybrids as controlled release systems. *Colloids Surfaces B*  
576 *Biointerfaces* 176, 249–255. <https://doi.org/10.1016/j.colsurfb.2018.12.030>
- 577 Changchaivong, S., Khaodhiar, S., 2009. Adsorption of naphthalene and phenanthrene on  
578 dodecylpyridinium-modified bentonite. *Appl. Clay Sci.* 43, 317–321.  
579 <https://doi.org/10.1016/j.clay.2008.09.012>
- 580 Chen, B., Zhu, L., Zhu, J., Xing, B., 2005. Configurations of the bentonite-sorbed  
581 myristylpyridinium cation and their influences on the uptake of organic compounds.  
582 *Environ. Sci. Technol.* 39, 6093–6100. <https://doi.org/10.1021/es0502674>
- 583 Chien, S.H., Clayton, W.R., 1984. Application of Elovich equation to the kinetics of  
584 phosphate release and sorption in soils<sup>1</sup>. *Soil Sci. Soc. Am. J.* 44, 265–268.  
585 <https://doi.org/10.2136/sssaj1980.03615995004400020013x>
- 586 Chitrakar, R., Makita, Y., Hirotsu, T., Sonoda, A., 2012. Montmorillonite modified with  
587 hexadecylpyridinium chloride as highly efficient anion exchanger for perchlorate ion.  
588 *Chem. Eng. J.* 191, 141–146. <https://doi.org/10.1016/j.cej.2012.02.085>
- 589 França, D.B., Torres, S.M., Filho, E.C.S., Fonseca, M.G., Jaber, M., 2019. Understanding the  
590 interactions between ranitidine and magadiite: Influence of the interlayer cation.  
591 *Chemosphere* 222, 980–990. <https://doi.org/10.1016/j.chemosphere.2019.01.154>
- 592 Freundlich, H.M.F., 1906. Over the adsorption in solution. *J. Phys. Chem.* 57, 385–471.
- 593 Ghemit, R., Makhloufi, A., Djebri, N., Fililissa, A., Zerroual, L., Boutahala, M., 2019.  
594 Adsorptive removal of diclofenac and ibuprofen from aqueous solution by  
595 organobentonites: Study in single and binary systems. *Groundw. Sustain. Dev.* 8, 520–  
596 529. <https://doi.org/10.1016/J.GSD.2019.02.004>
- 597 Greenland, D.J., Quirk, J.P., 1962. Adsorption of 1-n-alkyl pyridinium bromides by  
598 montmorillonite. *Clays Clay Miner.* 9, 484–499.
- 599 Gu, Z., Gao, M., Luo, Z., Lu, L., Ye, Y., Liu, Y., 2014. Bis-pyridinium dibromides modified  
600 organo-bentonite for the removal of aniline from wastewater : A positive role of  $\pi$ - $\pi$   
601 polar interaction. *Appl. Surf. Sci.* 290, 107–115.  
602 <https://doi.org/10.1016/j.apsusc.2013.11.008>
- 603 He, B., Wang, J., Liu, J., Hu, X., 2017. Eco-pharmacovigilance of non-steroidal anti-  
604 inflammatory drugs: Necessity and opportunities. *Chemosphere* 181, 178–189.  
605 <https://doi.org/10.1016/J.CHEMOSPHERE.2017.04.084>

- 606 He, H., Ma, L., Zhu, J., Frost, R.L., Theng, B.K.G., Bergaya, F., 2014. Synthesis of  
607 organoclays: A critical review and some unresolved issues. *Appl. Clay Sci.* 100, 22–28.  
608 <https://doi.org/10.1016/j.clay.2014.02.008>
- 609 Herrera, P., Burghardt, R., Huebner, H.J., Phillips, T.D., 2004. The efficacy of sand-  
610 immobilized organoclays as filtration bed materials for bacteria. *Food Microbiol.* 21, 1–  
611 10. [https://doi.org/10.1016/S0740-0020\(03\)00050-9](https://doi.org/10.1016/S0740-0020(03)00050-9)
- 612 Herrera, P., Burghardt, R.C., Phillips, T.D., 2000. Adsorption of *Salmonella enteritidis* by  
613 cetylpyridinium-exchanged montmorillonite clays. *Vet. Microbiol.* 74, 259–272.  
614 [https://doi.org/10.1016/S0378-1135\(00\)00157-7](https://doi.org/10.1016/S0378-1135(00)00157-7)
- 615 Ho, Y.S., McKay, G., 1999. Pseudo-second order model for sorption processes. *Process*  
616 *Biochem.* 34, 451–465. [https://doi.org/10.1016/S0032-9592\(98\)00112-5](https://doi.org/10.1016/S0032-9592(98)00112-5)
- 617 Ilescu, T., Baia, M., Kiefer, W., 2004. FT-Raman, surface-enhanced Raman spectroscopy  
618 and theoretical investigations of diclofenac sodium. *Chem. Phys.* 298, 167–174.  
619 <https://doi.org/10.1016/J.CHEMPHYS.2003.11.018>
- 620 Jović-Jovičić, N., Mojović, M., Stanković, D., Nedić-Vasiljević, B., Milutinović-Nikolić, A.,  
621 Banković, P., Mojović, Z., 2019. Characterization and electrochemical properties of  
622 organomodified and corresponding derived carbonized clay. *Electrochim. Acta* 296,  
623 387–396. <https://doi.org/10.1016/J.ELECTACTA.2018.11.031>
- 624 Karaman, R., Khamis, M., Quried, M., Halabieh, R., Makharzeh, I., Manassra, A., Abbadi, J.,  
625 Qtait, A., Bufod, S.A., Nasser, A., Nir, S., 2012. Removal of diclofenac potassium from  
626 wastewater using clay-micelle complex. *Environ. Technol.* 33, 1279–1287.  
627 <https://doi.org/10.1080/09593330.2011.619582>
- 628 Ke, Y.L., Jiao, L.F., Song, Z.H., Xiao, K., Lai, T.M., Lu, J.J., Hu, C.H., 2014. Effects of  
629 cetylpyridinium-montmorillonite, as alternative to antibiotic, on the growth performance,  
630 intestinal microflora and mucosal architecture of weaned pigs. *Anim. Feed Sci. Technol.*  
631 198, 257–262. <https://doi.org/10.1016/j.anifeedsci.2014.10.010>
- 632 Klaudia, Ś., Szaniawska, A., Caban, M., 2019. Evaluation of bioconcentration and  
633 metabolism of diclofenac in mussels *Mytilus trossulus* - laboratory study. *Mar. Pollut.*  
634 *Bull. J.* 141, 249–255. <https://doi.org/10.1016/j.marpolbul.2019.02.050>
- 635 Kovala-Demertzi, D., Dimitris, M., Terzis, A., 1993. Metal complexes of the anti-  
636 inflammatory drug sodium [2-[(2, 6-dichlorophenyl) amino] phenyl] acetate (diclofenac  
637 sodium). Molecular and crystal structure of cadmium diclofenac. *Polyhedron* 12, 1361–  
638 1370. [https://doi.org/10.1016/S0277-5387\(00\)84327-2](https://doi.org/10.1016/S0277-5387(00)84327-2)
- 639 Lagaly, G., Ogawa, M., Dékány, I., 2013. Clay mineral–organic interactions, in: Bergaya, F.,  
640 Lagaly, G. (Eds.), *Handbook of Clay Science*. Elsevier, *Developments in Clay Science*,  
641 Amsterdam, p. 435–505 (Chapter 10.3). <https://doi.org/10.1016/B978-0-08-098258-8.00015-8>
- 643 Lagergren, S., 1898. Zur theorie der sogenannten adsorption gelöster kungliga svenska  
644 vetenskapsakdemien. *Handlingar* 24, 1–39.
- 645 Langmuir, I., 1918. The adsorption of gases on plane surfaces of glass mica and platinum. *J.*  
646 *Am. Chem. Soc.* 40, 1361–1403. <https://doi.org/10.1021/ja02242a004>

- 647 Li, J., Zhu, L., Cai, W., 2006. Characteristics of organobentonite prepared by microwave as a  
648 sorbent to organic contaminants in water. *Colloids Surfaces A Physicochem. Eng. Asp.*  
649 281, 177–183. <https://doi.org/10.1016/j.colsurfa.2006.02.055>
- 650 Lima, É.C., Adebayo, M.A., Machado, F.M., 2015. Kinetic and Equilibrium Models of  
651 Adsorption, in: Bergmann, C.P., Machado, F.M. (Eds.), *Carbon Nanomaterials as*  
652 *Adsorbents for Environmental and Biological Applications*. Springer, Cham, pp. 33–69.  
653 [https://doi.org/10.1007/978-3-319-18875-1\\_3](https://doi.org/10.1007/978-3-319-18875-1_3)
- 654 Lin-Vien, D., Colthup, N.B., Fateley, W.G., Grasselli, J.G., 1991. *The Handbook of infrared*  
655 *and raman characteristic frequencies of organic molecules*, first. ed. Academic Press.
- 656 Lonappan, L., Kaur, S., Kumar, R., Verma, M., Surampalli, R.Y., 2016. Diclofenac and its  
657 transformation products : Environmental occurrence and toxicity - A review. *Environ.*  
658 *Int.* 96, 127–138. <https://doi.org/10.1016/j.envint.2016.09.014>
- 659 Luo, W., Hirajima, T., Sasaki, K., 2016. Optimization of hexadecylpyridinium-modified  
660 montmorillonite for removal of perchlorate based on adsorption mechanisms. *Appl. Clay*  
661 *Sci.* 123, 29–36. <https://doi.org/10.1016/j.clay.2016.01.005>
- 662 Luo, W., Inoue, A., Hirajima, T., Sasaki, K., 2017. Synergistic effect of  $\text{Sr}^{2+}$  and  $\text{ReO}_4^-$   
663 adsorption on hexadecyl pyridinium-modified montmorillonite. *Appl. Surf. Sci.* 394,  
664 431–439. <https://doi.org/10.1016/j.apsusc.2016.10.135>
- 665 Luo, W., Sasaki, K., Hirajima, T., 2018. Influence of the pre-dispersion of montmorillonite on  
666 organic modification and the adsorption of perchlorate and methyl red anions. *Appl.*  
667 *Clay Sci.* 154, 1–9. <https://doi.org/10.1016/j.clay.2017.12.032>
- 668 Luo, Z., Gao, M., Yang, S., Yang, Q., 2015. Adsorption of phenols on reduced-charge  
669 montmorillonites modified by bispyridinium dibromides: Mechanism , kinetics and  
670 thermodynamics studies. *Colloids Surfaces A Physicochem. Eng. Asp.* 482, 222–230.  
671 <https://doi.org/10.1016/j.colsurfa.2015.05.014>
- 672 Maia, G.S., Andrade, J.R., Silva, M.G.C., Vieira, M.G.A., 2019. Adsorption of diclofenac  
673 sodium onto commercial organoclay: Kinetic, equilibrium and thermodynamic study.  
674 *Powder Technol.* 345, 140–150. <https://doi.org/10.1016/j.powtec.2018.12.097>
- 675 Malachová, K., Praus, P., Pavlíčková, Z., Turicová, M., 2009. Activity of antibacterial  
676 compounds immobilised on montmorillonite. *Appl. Clay Sci.* 43, 364–368.  
677 <https://doi.org/10.1016/J.CLAY.2008.11.003>
- 678 Martinez-Costa, J.I., Leyva-Ramos, R., Padilla-Ortega, E., 2018. Sorption of diclofenac from  
679 aqueous solution on an organobentonite and adsorption of cadmium on organobentonite  
680 saturated with diclofenac. *Clays Clay Miner.* 66, 515–528.  
681 <https://doi.org/10.1346/ccmn.2018.064119>
- 682 Meleshyn, A., Bunnenberg, C., 2006. Interlayer expansion and mechanisms of anion sorption  
683 of Na-montmorillonite modified by cetylpyridinium chloride: A Monte Carlo study. *J.*  
684 *Phys. Chem. B* 110, 2271–2277. <https://doi.org/10.1021/jp056178v>
- 685 Momina, Shahadat, M., Isamil, S., 2018. Regeneration performance of clay-based adsorbents  
686 for the removal of industrial dyes: A review. *RSC Adv.* 8, 24571–24587.  
687 <https://doi.org/10.1039/c8ra04290j>

- 688 Moreno-González, R., Rodríguez-Mozaz, S., Huerta, B., Barceló, D., León, V.M., 2016. Do  
689 pharmaceuticals bioaccumulate in marine molluscs and fish from a coastal lagoon?  
690 *Environ. Res.* 146, 282–298. <https://doi.org/10.1016/J.ENVRES.2016.01.001>
- 691 Mugunthan, E., Saidutta, M.B., Jagadeeshbabu, P.E., 2018. Visible light assisted  
692 photocatalytic degradation of diclofenac using TiO<sub>2</sub>-WO<sub>3</sub> mixed oxide catalysts.  
693 *Environ. Nanotechnology, Monit. Manag.* 10, 322–330.  
694 <https://doi.org/10.1016/J.ENMM.2018.07.012>
- 695 Muñoz-Shugulí, C., Rodríguez, F.J., Bruna, J.E., Galotto, M.J., Sarantópoulos, C., Favaro  
696 Perez, M.A., Padula, M., 2019. Cetylpyridinium bromide-modified montmorillonite as  
697 filler in low density polyethylene nanocomposite films. *Appl. Clay Sci.* 168, 203–210.  
698 <https://doi.org/10.1016/j.clay.2018.10.020>
- 699 Oaks, J.L., Gilbert, M., Virani, M.Z., Watson, R.T., Meteyer, C.U., Rideout, B.A.,  
700 Shivaprasad, H.L., Ahmed, S., Iqbal Chaudhry, M.J., Arshad, M., Mahmood, S., Ali, A.,  
701 Ahmed Khan, A., 2004. Diclofenac residues as the cause of vulture population decline in  
702 Pakistan. *Nature* 427, 630–633. <https://doi.org/10.1038/nature02317>
- 703 Oliveira, T. De, Guégan, R., Thiebault, T., Le, C., Muller, F., Teixeira, V., Giovanela, M.,  
704 Boussafir, M., 2017. Adsorption of diclofenac onto organoclays: Effects of surfactant  
705 and environmental (pH and temperature) conditions. *J. Hazard. Mater.* 323, 558–566.  
706 <https://doi.org/10.1016/j.jhazmat.2016.05.001>
- 707 Oliveira, T., Guégan, R., 2016. Coupled organoclay/micelle action for the adsorption of  
708 diclofenac. *Environ. Sci. Technol.* 50, 10209–10215.  
709 <https://doi.org/10.1021/acs.est.6b03393>
- 710 Özdemir, G., Yapar, S., Limoncu, M.H., 2013. Preparation of cetylpyridinium  
711 montmorillonite for antibacterial applications. *Appl. Clay Sci.* 72, 201–205.  
712 <https://doi.org/10.1016/j.clay.2013.01.010>
- 713 Pérez-Estrada, L.A., Malato, S., Gernjak, W., Agüera, A., Thurman, E.M., Ferrer, I.,  
714 Fernández-Alba, A.R., 2005. Photo-fenton degradation of diclofenac: Identification of  
715 main intermediates and degradation pathway. *Environ. Sci. Technol.* 39, 8300–8306.  
716 <https://doi.org/10.1021/ES050794N>
- 717 Queiroga, L.N.F., Pereira, M.B.B., Silva, L.S., Silva Filho, E.C., Santos, I.M.G., Fonseca,  
718 M.G., Georgelin, T., Jaber, M., 2019. Microwave bentonite silylation for dye removal:  
719 Influence of the solvent. *Appl. Clay Sci.* 168, 478–487.  
720 <https://doi.org/10.1016/j.clay.2018.11.027>
- 721 Sarkar, B., Megharaj, M., Shanmuganathan, D., Naidu, R., 2013. Toxicity of organoclays to  
722 microbial processes and earthworm survival in soils. *J. Hazard. Mater.* 261, 793–800.  
723 <https://doi.org/10.1016/J.JHAZMAT.2012.11.061>
- 724 Schampera, B., Dultz, S., 2009. Determination of diffusive transport in HDPy-  
725 montmorillonite by H<sub>2</sub>O-D<sub>2</sub>O exchange using in situ ATR-FTIR spectroscopy. *Clay  
726 Miner.* 44, 249–266. <https://doi.org/10.1180/claymin.2009.044.2.249>
- 727 Scheurell, M., Franke, S., Shah, R.M., Hühnerfuss, H., 2009. Occurrence of diclofenac and its  
728 metabolites in surface water and effluent samples from Karachi, Pakistan. *Chemosphere*  
729 77, 870–876. <https://doi.org/10.1016/J.CHEMOSPHERE.2009.07.066>

- 730 Skoog, D.A., West, D.M., Holler, F.J., Crouch, S.R., 2012. Fundamentals of analytical  
731 chemistry.
- 732 Slaný, M., Jankovič, L., Madejová, J., 2019. Structural characterization of organo-  
733 montmorillonites prepared from a series of primary alkylamines salts: Mid-IR and near-  
734 IR study. *Appl. Clay Sci.* 176, 11–20. <https://doi.org/10.1016/j.clay.2019.04.016>
- 735 Starling, M.C.V.M., Amorim, C.C., Leão, M.M.D., 2019. Occurrence, control and fate of  
736 contaminants of emerging concern in environmental compartments in Brazil. *J. Hazard.  
737 Mater.* 372, 17–36. <https://doi.org/10.1016/J.JHAZMAT.2018.04.043>
- 738 Sun, K., Shi, Y., Chen, H., Wang, X., Li, Z., 2017a. Extending surfactant-modified 2:1 clay  
739 minerals for the uptake and removal of diclofenac from water. *J. Hazard. Mater.* 323,  
740 567–574. <https://doi.org/10.1016/j.jhazmat.2016.05.038>
- 741 Sun, K., Shi, Y., Wang, X., Li, Z., 2017b. Sorption and retention of diclofenac on zeolite in  
742 the presence of cationic surfactant. *J. Hazard. Mater.* 323, 584–592.  
743 <https://doi.org/10.1016/j.jhazmat.2016.08.026>
- 744 Sun, K., Shi, Y., Wang, X., Rasmussen, J., Li, Z., Zhu, J., 2017c. Organokaolin for the uptake  
745 of pharmaceuticals diclofenac and chloramphenicol from water. *Chem. Eng. J.* 330,  
746 1128–1136. <https://doi.org/10.1016/j.cej.2017.08.057>
- 747 Temkin, M.J., Pyzhev, V., 1940. Recent modifications to Langmuir isotherms. *Acta  
748 Physicochim. USSR* 12, 217–222.
- 749 Teppen, B.J., Aggarwal, V., 2007. Thermodynamics of organic cation exchange selectivity in  
750 smectites. *Clays Clay Miner.* 55, 119–130. <https://doi.org/10.1346/CCMN.2007.0550201>
- 751 Thanhmingliana, D.T., 2015. Efficient use of hybrid materials in the remediation of aquatic  
752 environment contaminated with micro-pollutant diclofenac sodium. *Chem. Eng. J.* 263,  
753 364–373. <https://doi.org/10.1016/j.cej.2014.10.102>
- 754 Vieno, N., Sillanpää, M., 2014. Fate of diclofenac in municipal wastewater treatment plant —  
755 A review. *Environ. Int.* 69, 28–39. <https://doi.org/10.1016/J.ENVINT.2014.03.021>
- 756 Volzone, C., Rinaldi, J.O., Ortiga, J., 2002. N<sub>2</sub> and CO<sub>2</sub> Adsorption by TMA-and HDP-  
757 Montmorillonites. *Mater. Res.* 5, 475–479. [https://doi.org/10.1590/S1516-  
758 14392002000400013](https://doi.org/10.1590/S1516-14392002000400013)
- 759 Witthuhn, B., Klauth, P., Klumpp, E., Narres, H.D., Martinius, H., 2005. Sorption and  
760 biodegradation of 2,4-dichlorophenol in the presence of organoclays. *Appl. Clay Sci.* 28,  
761 55–66. <https://doi.org/10.1016/j.clay.2004.01.003>
- 762 Yang, Q., Gao, M., Luo, Z., Yang, S., 2016. Enhanced removal of bisphenol A from aqueous  
763 solution by organo-montmorillonites modified with novel Gemini pyridinium surfactants  
764 containing long alkyl chain. *Chem. Eng. J.* 285, 27–38.  
765 <https://doi.org/10.1016/j.cej.2015.09.114>
- 766 Yapar, S., 2009. Physicochemical study of microwave-synthesized organoclays. *Colloids  
767 Surfaces A Physicochem. Eng. Asp.* 345, 75–81.  
768 <https://doi.org/10.1016/j.colsurfa.2009.04.032>
- 769 Zhu, L., Tian, S., Shi, Y., 2005. Adsorption of volatile organic compounds onto porous clay

770 heterostructures based on spent organobentonites. *Clays Clay Miner.* 53, 123–136.  
771 <https://doi.org/10.1346/CCMN.2005.0530202>

772 Zhuang, G., Zhang, Z., Jaber, M., 2019. Organoclays used as colloidal and rheological  
773 additives in oil-based drilling fluids: An overview. *Appl. Clay Sci.* 177, 63–81.  
774 <https://doi.org/10.1016/J.CLAY.2019.05.006>

775 Zhuang, G., Zhang, Z., Peng, S., Gao, J., Jaber, M., 2018. Enhancing the rheological  
776 properties and thermal stability of oil-based drilling fluids by synergetic use of organo-  
777 montmorillonite and organo-sepiolite. *Appl. Clay Sci.* 161, 505–512.  
778 <https://doi.org/10.1016/J.CLAY.2018.05.018>

779

780

781

782

783

784

785

786

787

788

## 789 **Figure captions**

790

791 Figure 1 - Equilibrium isotherms and their fitting to the Langmuir, Freundlich and Temkin  
792 models for sodium diclofenac adsorption on a) Bent-C<sub>12</sub>py-100%, (b) Bent-C<sub>16</sub>py-100%, (c)  
793 Bent-C<sub>12</sub>py-200% and (d) Bent-C<sub>16</sub>py-200% at 25 °C and pH 6.0.

794

795 Figure 2 – XRD patterns of organobentonites for (i) Bent-C<sub>12</sub>py-100%, (ii) Bent-C<sub>16</sub>py-100%,  
796 (iii) Bent-C<sub>12</sub>py-200% and (iv) Bent-C<sub>16</sub>py-200% (a) before and after diclofenac adsorption  
797 for hybrids prepared with initial drug concentrations of (b) 10 mg L<sup>-1</sup>, (c) 100 mg L<sup>-1</sup> and (d)  
798 500 mg L<sup>-1</sup>.

799  
800 Figure 3 – FTIR results for a) Bent-C<sub>16</sub>py-200% before and after diclofenac sorption using  
801 initial concentrations of b) 10 mg L<sup>-1</sup>, c) 100 mg L<sup>-1</sup> and d) 500 mg L<sup>-1</sup>; and e) free diclofenac  
802 sodium.

803

804 Figure 4 - Proposed scheme for diclofenac/organobentonite interaction, M = mechanism.

805

806

807

808

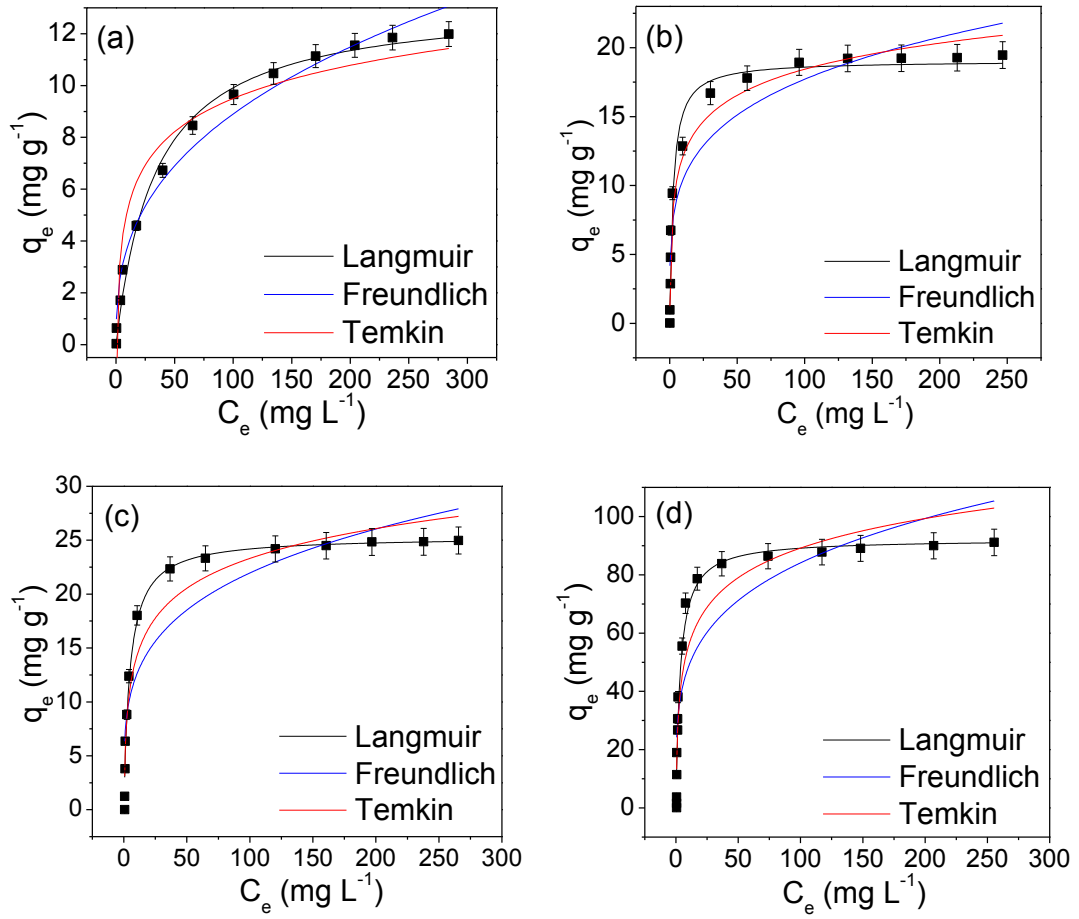
809

810

811

812

813



814 Figure 1

815

816

817

818

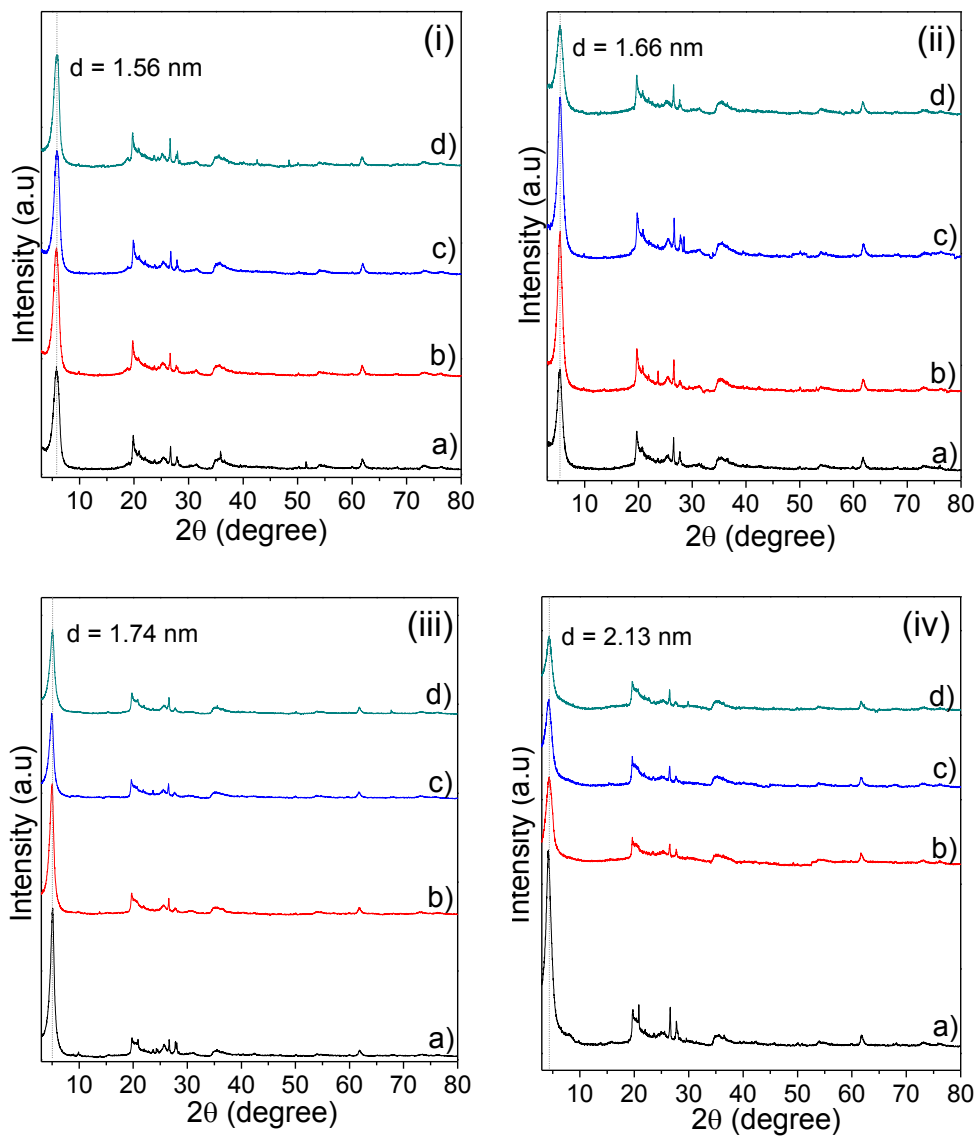
819

820

821

822





823

824

825 Figure 2

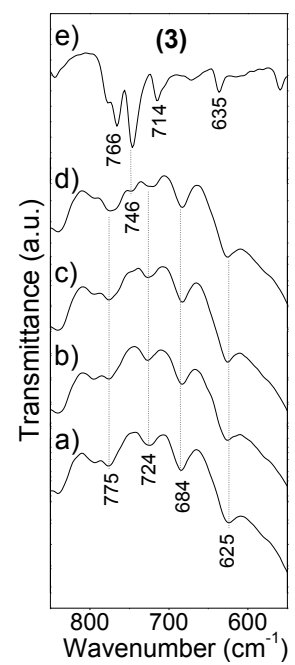
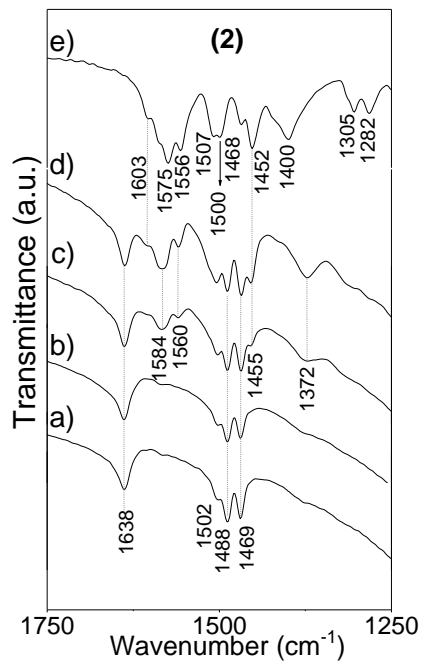
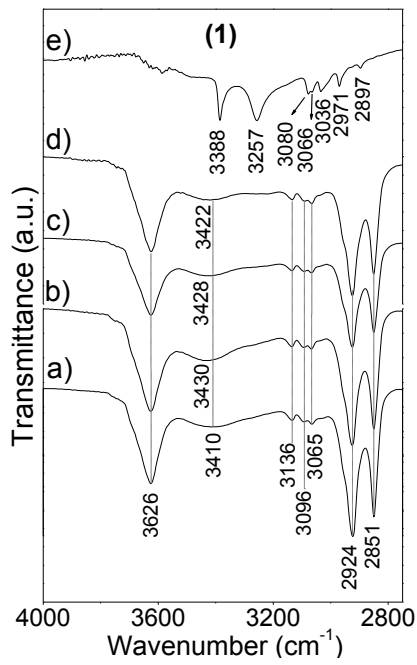
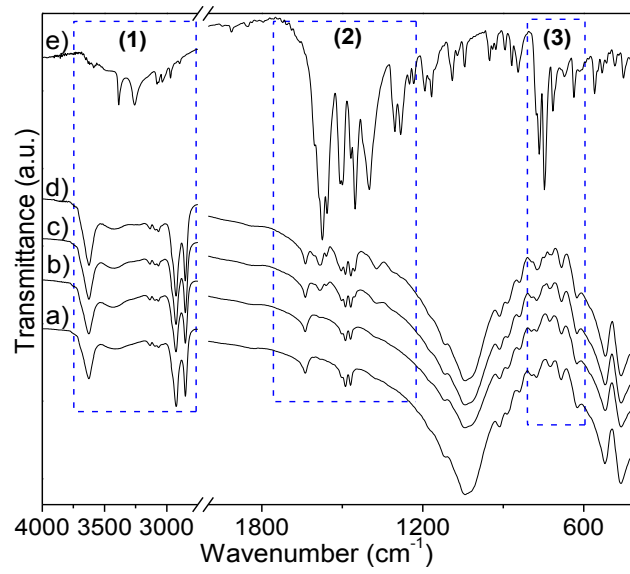
826

827

828

829

830



831

832 **Figure 3**

833

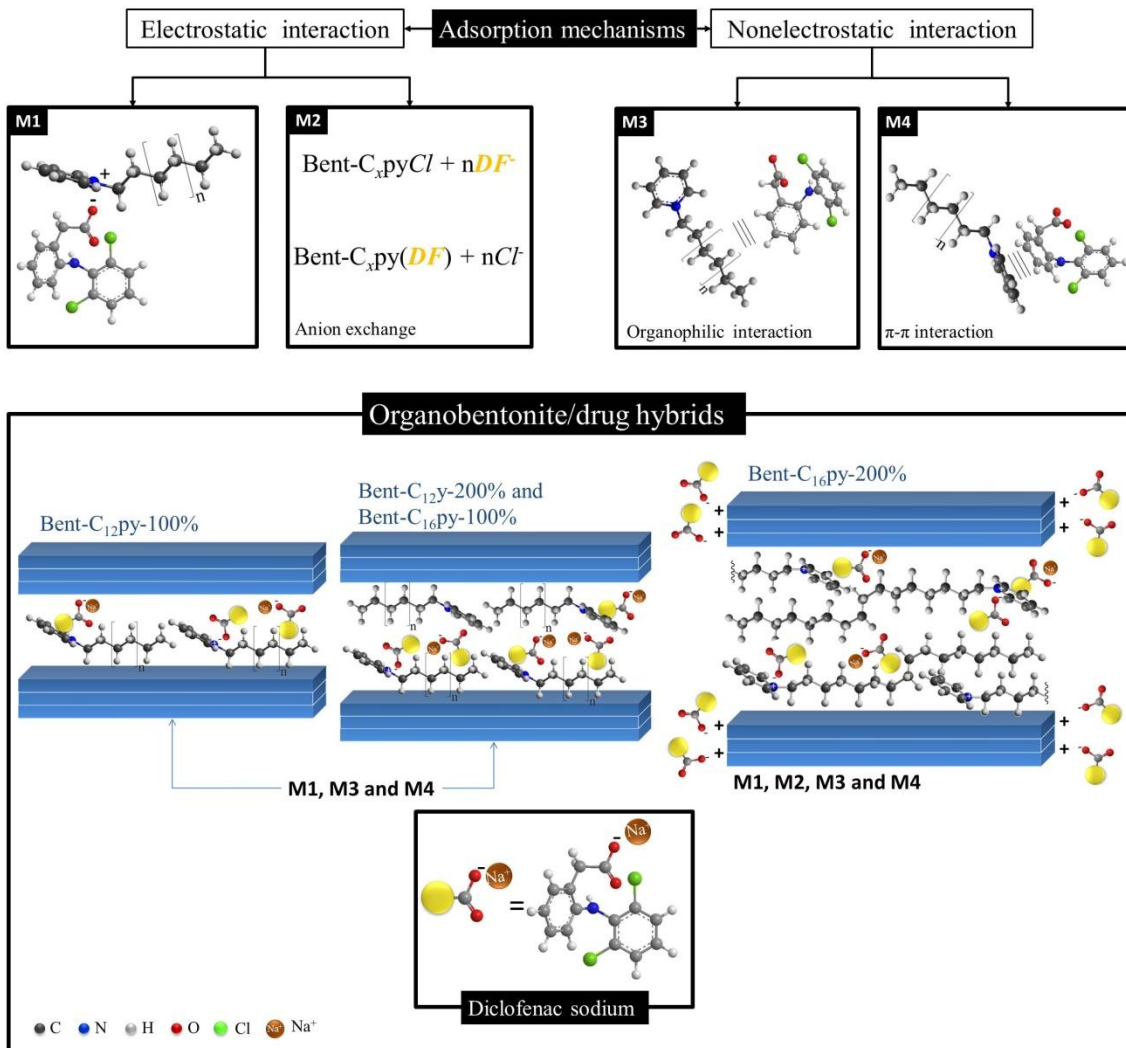
834

835

836

837

838



839

840 Figure 4

841

842

843

844

845

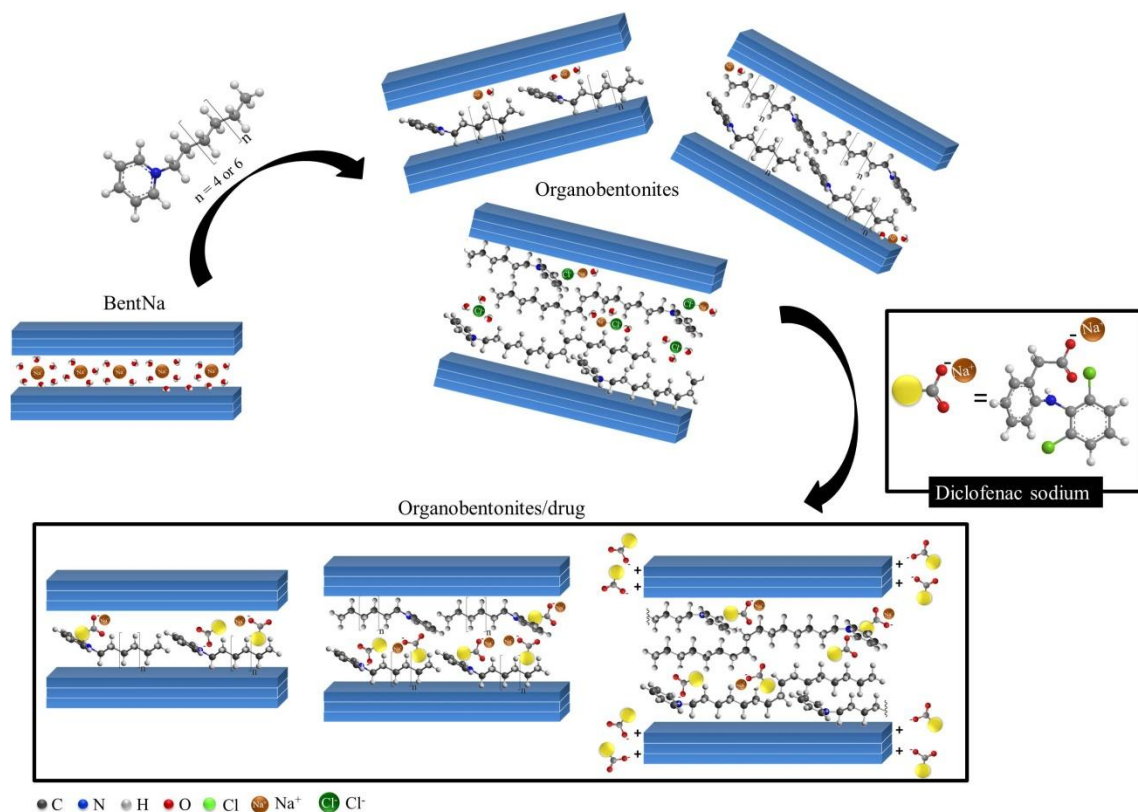
846

847

848

849

850 **Graphical abstract**



851

852

853

854

855

856

857

858

859

860

861 Table 1 – C, N and Cl elemental analysis of organobentonites and percentage of incorporated  
 862 surfactant in relation to the CEC of BentNa ( $\sigma_f$ ).

863

Sample	C		N		$\sigma_f$	Cl <sup>-</sup>
	%	mmol g <sup>-1</sup>	%	mmol g <sup>-1</sup>	%	mmol g <sup>-1</sup>
Bent-C <sub>12</sub> py-100%	12.30	10.25	0.93	0.66	89.0	*
Bent-C <sub>16</sub> py-100%	15.75	13.13	0.97	0.69	92.8	*
Bent-C <sub>12</sub> py-200%	14.85	12.38	0.98	0.70	93.3	*
Bent-C <sub>16</sub> py-200%	20.85	17.37	1.18	0.84	112.4	0.15 ± 0.01

864 \*null for all

865

866

867

868

869

870

871

872

873

874

875

876

877

878

879

880

881 Table 2 – Kinetic parameters obtained from the pseudo-first-order, pseudo-second-order and  
 882 Elovich equations in nonlinear fitting of diclofenac adsorption on organophilic bentonites  
 883 (Experimental conditions: 25 °C, pH 6.0 and 100 mg L<sup>-1</sup> diclofenac solution).

884

Pseudo-first-order					
Solid	q <sub>e(exp)</sub> (mg g <sup>-1</sup> )	k <sub>1</sub> (min <sup>-1</sup> )	q <sub>e(cal)</sub> (mg g <sup>-1</sup> )	R <sup>2</sup>	SD (mg g <sup>-1</sup> )
Bent-C <sub>12</sub> py-100%	5.50 ± 0.10	2.84 ± 0.65	5.01 ± 0.13	0.9242	0.410
Bent-C <sub>16</sub> py-100%	8.98 ± 0.27	3.54 ± 0.82	8.36 ± 0.20	0.9573	0.554
Bent-C <sub>12</sub> py-200%	12.98 ± 0.05	2.18 ± 0.12	12.80 ± 0.09	0.9938	0.293
Bent-C <sub>16</sub> py-200%	38.71 ± 0.04	4.06 ± 0.33	38.53 ± 0.27	0.9950	0.814
Pseudo-second-order					
Solid	q <sub>e(exp)</sub> (mg g <sup>-1</sup> )	k <sub>2</sub> (g mg <sup>-1</sup> min <sup>-1</sup> )	q <sub>e(cal)</sub> (mg g <sup>-1</sup> )	R <sup>2</sup>	SD (mg g <sup>-1</sup> )
Bent-C <sub>12</sub> py-100%	5.50 ± 0.10	0.99 ± 0.25	5.18 ± 0.11	0.9641	0.282
Bent-C <sub>16</sub> py-100%	8.98 ± 0.27	0.81 ± 0.25	8.54 ± 0.16	0.9752	0.422
Bent-C <sub>12</sub> py-200%	12.98 ± 0.05	0.35 ± 0.01	13.06 ± 0.05	0.9985	0.141
Bent-C <sub>16</sub> py-200%	38.71 ± 0.04	0.33 ± 0.02	38.95 ± 0.11	0.9993	0.308
Elovich					
Solid	α (10 <sup>6</sup> mg g <sup>-1</sup> min <sup>-1</sup> )	β (g mg <sup>-1</sup> )	R <sup>2</sup>	SD (mg g <sup>-1</sup> )	
Bent-C <sub>12</sub> py-100%	1.07 ± 0.66	3.56 ± 0.13	0.9983	0.061	
Bent-C <sub>16</sub> py-100%	44.5 ± 33.4	2.57 ± 0.09	0.9992	0.076	
Bent-C <sub>12</sub> py-200%	84.97 ± 377.04	1.73 ± 0.38	0.9622	0.727	
Bent-C <sub>16</sub> py-200%	9.48 10 <sup>15</sup> ± 133.78 10 <sup>15</sup>	1.40 ± 0.37	0.9915	1.061	

885

886

887 Table 3 – Adsorption parameters of diclofenac on organophilic bentonites at 25 °C and pH 6.0  
 888 according to the Langmuir, Freundlich and Temkin models.

889

Langmuir					
Solid	$q_e$ (exp)	$q_{max}$	$K_L$	$R^2$	SD
	( $mg\ g^{-1}$ )	( $mg\ g^{-1}$ )	( $10^{-1}\ L\ mg^{-1}$ )		( $mg\ g^{-1}$ )
Bent-C <sub>12</sub> py-100%	13.02 ± 0.65	13.26 ± 0.35	0.30 ± 0.03	0.9917	0.41
Bent-C <sub>16</sub> py-100%	19.30 ± 0.96	19.05 ± 0.43	4.00 ± 0.56	0.9806	1.05
Bent-C <sub>12</sub> py-200%	25.50 ± 1.02	25.33 ± 0.53	2.11 ± 0.24	0.9843	1.23
Bent-C <sub>16</sub> py-200%	91.13 ± 1.82	92.20 ± 2.68	2.91 ± 0.39	0.9704	6.15
Freundlich					
Solid	n	$K_f$	$R^2$	SD	
		( $mg\ g^{-1})(mg\ L^{-1})^{-1/n}$ )		(mg g <sup>-1</sup> )	
Bent-C <sub>12</sub> py-100%	2.71 ± 0.21	1.63 ± 0.23	0.9767	0.70	
Bent-C <sub>16</sub> py-100%	4.37 ± 0.60	6.17 ± 0.91	0.8943	2.47	
Bent-C <sub>12</sub> py-200%	4.10 ± 0.65	7.10 ± 1.33	0.8533	3.76	
Bent-C <sub>16</sub> py-200%	4.16 ± 0.67	27.82 ± 4.81	0.7961	16.14	
Temkin					
Solid	$b_T$	$A_T$	$R^2$	SD	
	( $10^2\ J\ mol^{-1}$ )	( $L\ mg^{-1}$ )		(mg g <sup>-1</sup> )	
Bent-C <sub>12</sub> py-100%	13.61 ± 1.02	1.70 ± 0.56	0.9366	1.31	
Bent-C <sub>16</sub> py-100%	9.22 ± 0.40	8.60 ± 1.90	0.9766	1.16	
Bent-C <sub>12</sub> py-200%	6.20 ± 0.40	3.43 ± 0.99	0.9498	2.20	
Bent-C <sub>16</sub> py-200%	1.70 ± 0.13	4.41 ± 1.38	0.9156	10.38	

890